The Use of the Lamellar Phase for the Construction of Reagentless Biosensors Based on NAD^+ Dependent Glutamate Dehydrogenase.

Valeri Pavlov[1], Britta Lindholm-Sethson[2], Goran Lindblom[2], Ioanis Katakis[1]*

[1]Bioanalysis and Bioelectrochemistry Group, Chemical Engineering, Universitat Rovira i Virgili, E-43006, Tarragona (Catalonia), Spain. [2]Department of Chemistry, Umeå University, Umeå, SE-901 87, Sweden.
Tel: +34 977 55 9655. Fax: +34 977 55 9667. E-mail: ioanis.katakis@urv.net

A new NADH oxidizing redox surfactant [Os(1,10-phenanthroline-5,6-dione)$_2$(4,4´-[$CH_3(CH_2)_{17}NHCO]_2$bpy)]$(PF_6)_2$ (Os-phendione-surfactant) has been synthesized. The study of its tensoactive behaviour in a Langmuir-Blodgett trough demonstrated high stability of the resulting monolayer on the water-air interface and mean molecular area from 170 to 230 Å. The lamellar phase suspension based on the lipid 1,2-dioleoyl-sn-glycero-3-phosphatidylcholine containing Os-phendione-surfactant, NAD^+ and bovine glutamate dehydrogenase was prepared and immobilized on graphite electrodes to yield reagentless biosensors operating at low applied potential of 150 mV *vs*. Ag/AgCl/KCl_{sat}. Their response curves and dependence of the response current on temperature and pH have been studied in order to determine the rate limiting factor. The operational half-life time of these sensors was 0.5 h.

Keywords: glutamate analysis, glutamate dehydrogenase, reagentless biosensors, NAD^+, amphiphilic mediator

* To whom the correspondence should be addressed

Amphiphilic compounds or surfactants form micelles, liposomes, vesicles and lamellar phase in liquids and monolayers in gas-liquid interface, which can be transferred to solid substrates by Langmiur-Blodgett (LB) techniques. The development of inorganometallic surfactants serving as electron transfer reagents has been mentioned in the literature. Tensoactive bipyridine complexes of ruthenium were synthesised and their LB films were transferred on glass substrates for the photo-generation of hydrogen from water.[1,2] These redox active amphiphilic complexes can be utilized in electrochemical biosensors for the mediation of enzymes. For example, surfactants derived from bipyridine complexes of osmium and ruthenium,[3,4] and ferrocene[5,6] demonstrated capacity for the exchange of electrons with the active centre of glucose oxidase.

Another class of amphiphilic molecules are lipids, which form cell membranes, also can be used in biosensors for immobilization of proteins on solid substrates. There are two basic ways for the membrane creation: the transfer a monolayer from the liquid-gas interface using the Langmuir –Blodgett technique and vesicle spreading.[7] In both methods the inner monolayer can be deposited by the LB method or attached to the substrate surface by self-assembly from a solution through forming covalent bonds of alkyl mercaptanes on gold and alkyl silanes on silicon surfaces [8,9] or through ion bridges.[10] The advantages of the LB techniques are easy automation of the process and easy optical following by imaging ellipsometry or microfluorescence.[11,12] In addition, by choosing different lipid mixtures and thermodynamic conditions one can deposit alternating layers with different microstructures. Vesicle spreading is based on the electrostatical or covalent linking of vesicles under high tension to the substrate surface followed by their spreading and collapse.[13] Vesicle spreading proceeds through two mechanisms: the advancement of single bilayers, resulting in incomplete coverage, or viscous fingerlike spreading of giant vesicles leading to closed bilayers by self-healing. The resulting solid-supported lipid bilayers are model systems for biological membranes[7] but they can incorporate membrane proteins only if the lipid bilayers are separated from the solid support by polymer spacer groups such as poly(oxyethylene).[14] Membrane proteins can be incorporated in lipid bilayers by the transfer of a mixed monolayer containing proteins and lipids on a solid support us LB techniques but the serious drawback of this method is the requirement to dissolve lipids and a protein in organic solvent before spreading on the water-air interface, which may denature proteins. Hence the alternative method based on the fusion of liposomes and vesicles containing membrane proteins in lipid bilayers have been developed. It was successfully used in case of cytochrome c oxidase,[15,16,17] and H^+-ATPase,[18] acetylcholine receptor.[19] The majority of commercially available enzymes and coenzymes is hydrophilic so they can be incorporated only between hydrophilic sides of lipid bilayers. For example, vesicles containing encapsulated glucose oxidase were immobilized under a dialysis membrane on hydrogen peroxide electrodes to fabricate glucose biosensors with the increased linear range.[20,21] To our knowledge the fabrication of "reagentless" biosensors based on the immobilization of NAD^+ dependent dehydrogenases together with the cofactor in the lipid lamellar phase has never been reported. In this work we present "reagentless" biosensors based on bovine glutamate dehydrogenase (GLDH). Glutamate is a well known neurotransmitter, which plays important role in the development of neurological diseases such as amnesia, depression, and schizophrenia.[22,23] It is also a marker in the diagnosis of miocardic diseases and hepatitis.[24] In order to develop sensors based on NAD^+ dependent dehydrogenase we synthesized the new NADH oxidizing

amphiphilic complex of osmium with 1,10-phenanthroline-5,6-dione which allows to recycle NAD^+ at applied potential as low as 150 mV *vs*. $Ag/AgCl/KCl_{sat}$.

EXPERIMENTAL SECTION

Materials. GLDH (E.C. 1.4.1.3) from bovine liver, as suspension in saturated ammonium was purchased from Biozyme (UK), nicotinamide adenine nucleotide (NAD^+), L-glutamic acid monosodium salt, dimethylformamid (DMF), *n*-$C_{18}H_{37}NH_2$, sodium dihydrogen phosphate, sodium hydroxide, *ortho*-phosphoric acid, sodium chloride, thionyl chloride, NH_4PF_6, 2,2'-bipyridine-4,4'-dicarboxylic acid, absolute 1,4-dioxane were obtained from Sigma-Aldrich (USA), K_2OsCl_6 was from Alfa (Spain), ethylene glycol and sodium dithionite were obtained from Pancreac (Madrid, Spain), 1,2-dioleoyl-sn-glycero-3-phosphatidylcholine from Larodan Fine Chemicals (Sweden), 1,10-phenanthroline-5,6-dione was prepared by the published procedure.[25]

[Os(1,10-phenanthroline-5,6-dione)$_2$Cl$_2$] was synthesized according to the adapted method.[26] Generally the synthesis procedure involved refluxing of K_2OsCl_6 with 1,10-phenanthroline-5,6-dione in DMF under argon in the dark for 1 hr, followed by reduction with aqueous sodium dithionite solution.

Synthesis of 4,4´-[CH$_3$(CH$_2$)$_{17}$NHCO]$_2$bpy (I)

0.82 mmol of 2,2'-bipyridine-4,4'-dicarboxylic acid were refluxed during 24 h in 4 ml of thionyl chloride (Aldrich, USA), next thionyl chloride was evaporated under vacuum during 4 h. The reaction product was dissolved in 40 ml of absolute 1,4-dioxane. This solution was added dropwise to a solution 1.8 mmol of *n*-$C_{18}H_{37}NH_2$ in 200 ml of absolute 1,4-dioxane during 20 min, the reaction mixture was left to stay overnight. The next day the solid was filtered off, washed with 1,4-dioxane and airdried to give compound I.

Synthesis of [Os(1,10-phenanthroline-5,6-dione)$_2$(4,4´-[CH$_3$(CH$_2$)$_{17}$NHCO]$_2$bpy)](PF$_6$)$_2$ (II) (Os-phendione-surfactant)

0.1468 mmol of [Os(1,10-phenanthroline-5,6-dione)$_2$Cl$_2$] and 0.1762 mmol of compound I were refluxed during 1 h in 5 ml of deaerated ethylene glycol under argon in the dark. Next the product was precipitated by mixing with a solution of 1 g of NH_4PF_6 in 100 ml of water. The solid was filtered off and washed with water, extracted with acetone and air dried to yield compound II. The synthesis route is presented in Figure 2. ^{1}H NMR performed in $CDCl_3$ with a tetramethylsilane standard confirmed the presence of long alkane chains: 1.29 p. p. m. (m) 1.26 (m), 0.88 (t).

Preparation of bovine GLDH solution

In order to purify mesophilic bovine GLDH 4 ml of meso GLDH suspension in saturated ammonium sulphate solution were centrifuged during 10 min at 14000 RPM at 5°C. The precipitated enzyme was isolated from the ammonium sulfate solution and dissolved in 3 ml of 0.1 M sodium phosphate buffer (pH 7.4) containing 0.15 M

sodium chloride, next the resulting enzyme solution was extensively dialyzed at 5^{o}C against 200 ml of the same buffer during 24 h, the buffer solution being changed every two hours.

Preparation of graphite electrodes. Spectrographic graphite rods of 3 mm in diameter (Carbone of America, USA) were cut into pieces of 2 cm in longitude, introduced into heat-shrinkable PVC plastic tubes, shrunk by heating, wet polished on fine (grit 400 and 600) emery paper (Buehler, USA) and sonicated in water.

Preparation of reagentless glutamate biosensors based on immobilization between lipid bilayers. 1.5 mg of Os-phendione-surfactant and 10 mg of 1,2-dioleoyl-sn-glycero-3-phosphatiylcholine were dissolved in 0.5 mL of chloroform. Then this solution was evaporated under vacuum in a pear shaped flask to form the solid thin layer on the bottom. Next 1 mL of a solution containing 5.8 mg mL^{-1} (38 U mL^{-1} at 30^{o}C) of bovine glutamate dehydrogenase and 40 mg of NAD^{+} in 0.1 M phosphate buffer pH 7.6 were stirred during 2 h to form the lamellar phase. The suspension was washed 6 times with 1 mL of 0.1 M phosphate buffer (pH 7.6), using centrifugation at 4000 rpm during 10 min every time. Next the volume of this suspension was adjusted to 1 mL and 5 μL of it was deposited per graphite electrode and air-dried during 1 h.

Electrochemical measurements. A three-electrode conventional thermostabilised cell (3 mL) equipped with an Ag/AgCl/KCl_{sat} reference electrode, a platinum auxiliary electrode, and a graphite electrode modified according to one of the above mentioned methods as working electrode. The buffer, pH 7.4 (0.1 M sodium phosphate containing 0.15 M sodium chloride) served as supporting electrolyte. The response to successive additions of stock glutamate solution was registered as steady state current on a three-electrode potentiostat Autolab PGSTAT 10 (Eco chemie, Holland) controlled by a computer. The working potential was 150 mV vs. Ag/AgCl/KCl_{sat} and the temperature of a thoroughly stirred solution was 30^{o}C.

GLDH assay method. The activity of GLDH was tested spectrophotometrically by following the increase in absorbance at 340 nm 30^{o}C. The assay solution contained 5 mM NAD^{+} and 10 mM in 0.1 M sodium phosphate buffer (pH 7.4). The ΔA_{340} (Au/min) was obtained using the maximum linear rate for both the test and blank (without the enzyme) mixtures. The activity was calculated using ε_{NADH}=6.22 mM^{-1}cm^{-1} extinction coefficient of β-NADH. One unit of GLDH oxidizes 1 μmol of L-glutamate per minute at pH 7.4 at 30^{o}C. Protein concentration was determined spectrophotometrically at A_{280} using an absorbance coefficient of 0.973 cm^{2} mg^{-1}.

RESULTS AND DISCUSSION

Methods for the fabrication of reagentless glutamate biosensors. The glutamate biosensors presented hereby are based on the oxidation of L-glutamate by NAD^{+} through mesophilic and thermophilic glutamate dehydrogenase (GLDH) according to the reaction:

$$\text{L-glutamate} + NAD^+ + H_2O \overset{\text{GLDH}}{\rightleftarrows} \alpha\text{–ketoglutarate} + NADH + NH_4^+$$

with the equilibrium constant shifted to the formation of L-glutamate, nevertheless the reoxidation of NADH by Os-phendione-surfactant mediator, which is oxidized in its turn at the graphite surface of the electrode at low positive potential of 150 mV *vs.* Ag/AgCl/KCl_{sat}, displaces the equilibrium to the production of NADH. The sequence of chemical reactions in the glutamate biosensor is shown schematically in Figure 1. The immobilization of GLDH, NAD^+ and mediator is the necessary condition for design of reagentless glutamate biosensors. It was achieved by the formation of the lamellar phase suspension containing new NADH oxidizing surfactant (Os-phendione-surfactant), 1,2-dioleoyl-sn-glycero-3-phosphatiylcholine, NAD^+, and GLDH. The synthetic root to Os-phendione-surfactant can be seen in Figure 2. It was shown in the literature that complexes of transition metals with 1,10-phenanthroline-5,6-dione are stable mediators for the electrochemical oxidation of NADH,[27,28,29] therefore we converted [Os(1,10-phenanthroline-5,6-dione)$_2Cl_2$] complex into a surfactant by complexation with amphiphilic bipyridine (I). This compound has demonstrated tensoactivity and forms stable Langmuir monolayer on water-air interface in a Langmuir's trough. The surface pressure/area isotherm of this mediator is shown in Figure 3. The results obtained from this isotherm point out to mean molecular area from 170 to 230 $Å^{-2}$. This high value can be explained by the presence of bulky phenanthroline ligands. Some reorganization of a monolayer takes place starting from surface pressure value of 40 mN m^{-1}. The lamellar phase suspension was formed by mixing biosensor components with the lipid in an aqueous solution, next they were separated by centrifuge, adsorbed on the graphite electrode surface, and air-dried. ^{31}P NMR investigation was utilized to confirm the structures of the lamellar phase suspension in water and on the graphite surface. In both cases the NMR spectra showed the broad peak from –7 to –15 ppm, which is the strong indication to the presence of lamellar phase.

Electrocatalytical oxidation of L-glutamate. The reagentless glutamate biosensor demonstrated change in the CV behaviour when glutamate solution was injected into the cell (Figure 4). In the presence of glutamate clear electrocatalytic waves achieving almost a plateau at potentials more negative than 200 mV *vs.* Ag/AgCl/KCl_{sat} have been seen. Our previous study of the complex of [Os(1,10-phenanthroline-5,6-dione)$_2Cl_2$] with poly(4-vinylpyridine)[30] proved that the potential of 150 mV *vs.* Ag/AgCl/KCl_{sat} was sufficient for electrocatalytic oxidation of NADH hence the same potential was used in continuation of the work.

Effect of pH on the response of glutamate biosensors. The effect of the pH on the maximum response current of glutamate biosensors was studied in steady state mode using 0.1 M phosphate buffer, pH was adjusted

with aqueous solutions of 1 M NaOH or H_3PO_4. In Figure 5 it can be seen that the biosensors have maximum response at pH 9.0. This result is in good agreement with the pH optimum of 8.5-9.0 for glutamate oxidation by free bovine GLDH in the solution.[31] The complexes of osmium are unstable at the pH values higher than 8.0, at the same time, the controlled electrodes prepared without GLDH showed increase in non-specific oxidation of glutamate starting from pH 9.0, hence the pH of 7.4 was chosen for further experiments, because this is the physiologic value of the pH at which the analysis *in vivo* could be carried out.

Effect of temperature on the response of glutamate biosensors. The effect of temperature on the response of glutamate biosensors is presented in Figures 6. Vesicles based sensors demonstrated optimal temperature of 54°C. This data is in good agreement with the published thermostability study of bovine GLDH according to which this enzyme loses activity starting from the temperature of 52°C.[32] The activation energies for the glutamate biosensors were calculated from Arhenius plot obtained by plotting the logarithm of the relative response current against the reciprocal of the absolute temperature. The activation energy is 56.3 kJ mol^{-1}. Activation energies of the GLDH biosensors are significantly higher than the activation energy of free bovine GLDH, 12.9 kJ mol^{-1}.[32] This fact indicates that the response of the glutamate biosensors was not limited by the kinetics of glutamate oxidation with NAD^+ through GLDH.

Response curves and operational stability of the glutamate biosensors. The latest kinetic study into the mechanism of enzymatic deamination confirmed that bovine dehydrogenase has an ordered sequential mechanism of substrate binding preceded by complexation with NAD^+ [33] therefore the calculations of characteristics of the glucose sensors were based on the following modified kinetic model for the conversion of substrate B to product Q.[34] Figure 7 illustrates the kinetic scheme for the operation of reagentless biosensors based on the enzyme glutamate dehydrogenase (E) catalyzing the reaction of immobilized NAD^+ (A) with a L-glutamate (B) to give immobilized NADH (P), α–ketoglutarate (Q), and NH_4^+ (R). Then a mediator (M), which can stay in reduced (M_{red}) and oxidized (M_{ox}) forms, immobilized on the electrode surface catalyzes the electrochemical conversion of P back to A. A_{im} and P_{im} are the concentrations of immobilized A and P. B_o, Q_o, R_o are the concentrations of the substrate and the products in the lamellar phase B_∞, Q_∞ and R_∞ are the concentrations of the substrate and the products in the external medium. k'_B, k'_Q and k'_R are mass transfer coefficients of the substrate and the products (cm s^{-1}), respectively. L is the thickness of the hydrogel layer. The following expressions for the flux of B to the electrode surface (j_{el}), which determines the current density of a biosensor (j) through the equation $j = nFj_{el}$, where n is the number of exchanged electrons and F is the Faraday's constant, can be obtained.

$$j_{el} = k'_B(B_\infty - B_o) \quad (1)$$
$$j_{el} = L(k_1 A_{im}[E] - k_{-1}[E{\cdot}A]) \quad (2)$$
$$j_{el} = L(k_2 B_o[E{\cdot}A] - k_{-2}[E{\cdot}A{\cdot}B]) \quad (3)$$
$$j_{el} = L(k_3 [E{\cdot}A{\cdot}B] - k_{-3}[E{\cdot}P{\cdot}Q{\cdot}R]) \quad (4)$$
$$j_{el} = L(k_4 [E{\cdot}P{\cdot}Q{\cdot}R] - k_{-4}[E{\cdot}P{\cdot}Q]Q_o) \quad (5)$$
$$j_{el} = L(k_5 [E{\cdot}P{\cdot}Q] - k_{-5}[E{\cdot}P]Q_o) \quad (6)$$
$$j_{el} = L(k_6 [E{\cdot}P] - k_{-6}[E]P_{im}) \quad (7)$$
$$j_{el} = k'_Q Q_o \quad (8)$$

$$j_{el} = k'_R R_o \quad (9)$$

$$j_{el} = k_7 P_o \Gamma_{Mox} - k_{-7} \Gamma_{M\cdot P} \quad (10)$$

$$j_{el} = k_8 \Gamma_{M\cdot P} \quad (11)$$

$$j_{el} = k_9 \Gamma_{Mred} \quad (12)$$

$$E_t = [E] + [E\cdot A] + [E\cdot A\cdot B] + [E\cdot P\cdot Q\cdot R] + [E\cdot P\cdot Q] + [E\cdot P] \quad (13)$$

$$\Gamma_M = \Gamma_{M\cdot P} + \Gamma_{Mox} + \Gamma_{Mred} \quad (14)$$

$$A_t = A_{im} + P_{im} \quad (15)$$

Where Γ_{Mox} and Γ_{Mred} are the surface coverages of the mediator in oxidized and reduced forms, respectively. Γ_M is the total mediator surface coverage. $\Gamma_{M\cdot P}$ is the surface coverage of the intermediate complex between the mediator and NADH. A_t and E_t are the total concentrations of NAD^+ and the enzyme immobilized in the lamellar phase, respectively. The equations (1-15) yield the equation (16):

$$LV_1\Gamma_M k_{cat} E_t A_t B_\infty = j_{el}[K_{AB}\Gamma_M k_{cat} + K_B\Gamma_M k_{cat} A_t + K_A\Gamma_M k_{cat} B_\infty + A_t\Gamma_M k_{cat} B_\infty + LV_1(A_t + K_M)B_\infty + (LV_1 A_t \Gamma_M k_{cat})/k'_B] + j^2_{el}[(K_{PQ}K_B A_t \Gamma_M k_{cat})/(K_{iP}K_{iQ}K_R k'_R) - LV_1(A_t + K_M)/k'_B - K_{AB} - K_B(A_t + K_M) - K_A B_\infty + K_M K_{QR} K_{iA} K_B/(K_{iP}K_{iQ}K_R) - (A_t + K_M)B_\infty - A_t\Gamma_M k_{cat}/k'_B + \Gamma_M k_{cat} K_{PQ} K_{iA} K_B R_o/(K_{iP}K_{iQ}K_R k'_R) + K_A K_M B_\infty/K_{iP} + K_{iR}K_P K_B A_t B_\infty \Gamma_M k_{cat}/(K_{iB}K_{iP}K_{iQ}K_R k'_Q) + K_{PQ}K_B A_t B_\infty \Gamma_M k_{cat}/(K_{iB}K_{iP}K_{iQ}k'_R)] + j^3_{el}[LV_1 K_M/(K_{eq}k'_Q k'_R) + K_A/k'_B + (A_t + K_M)/k'_B - K_{PQ}K_{iA}K_B/(K_{iP}K_{iQ}K_R k'_R) + \Gamma_M k_{cat} K_P K_{iA} K_B/(K_{iP}K_{iQ}K_R k'_Q k'_R) + K_M K_R K_{iA} K_B/(K_{iP}K_{iQ}K_R k'_Q) + K_M K_P K_{iA} K_B/(K_{iP}K_{iQ}K_R k'_R) - K_A K_M/(K_{iP}k'_B) + K_A K_M B_\infty/(K_{iQ}K_{iP}k'_Q) - K_{iR}K_P K_B(A_t + K_M)B_\infty/(K_{iB}K_{iP}K_{iQ}K_R k'_Q) - K_{iR}K_P K_B A_t \Gamma_M k_{cat}/(K_{iB}K_{iP}K_{iQ}K_R k'_B k'_Q) + K_P K_B A_t \Gamma_M k_{cat}/(K_{iP}K_{iQ}K_R k'_Q k'_R) - K_{PQ}K_B(A_t + K_M)/(K_{iP}K_{iQ}K_R k'_R) + K_P K_B A_t B_\infty \Gamma_M k_{cat}/(K_{iB}K_{iP}K_{iQ}K_R k'_Q k'_R) - K_{PQ}K_B B_\infty(A_t + K_M)/(K_{iB}K_{iP}K_{iQ}K_R k'_R) - A_t\Gamma_M k_{cat} K_{PQ}K_B/(K_{iB}K_{iP}K_{iQ}K_R k'_B k'_R)] + j^4_{el}[K_{iA}K_B K_M/(K_{iP}K_{iQ}K_R k'_Q k'_R) - K_P K_{iA}K_B/(K_{iP}K_{iQ}K_R k'_Q k'_R) - K_A K_M/(K_{iQ}K_{iP}k'_B k'_Q) + K_{iR}K_P K_B(A_t + K_M)/(K_{iB}K_{iP}K_{iQ}K_R k'_B k'_Q) - K_P K_B(A_t + K_M)/(K_{iP}K_{iQ}K_R k'_Q k'_R) - K_P K_B B_\infty/(K_{iB}K_{iP}K_{iQ}K_R k'_Q k'_R) - K_P K_B A_t \Gamma_M k_{cat}/(K_{iB}K_{iP}K_{iQ}K_R k'_B k'_Q k'_R) + K_A B_\infty K_M/(K_{iR}K_{iP}K_{iQ}k'_Q k'_R) + K_{PQ}K_B(A_t + K_M)/(K_{iB}K_{iP}K_{iQ}K_R k'_B k'_R)] + j^5_{el}[K_P K_B(A_t + K_M)/(K_{iB}K_{iP}K_{iQ}K_R k'_B k'_Q k'_R) - K_A K_M/(K_{iR}K_{iP}K_{iQ}k'_B k'_Q k'_R)] \quad (16)$$

Where $V_1 = E_t(k_1k_2k_3k_4k_5k_6)/(k_1k_2k_5k_6k_{-3} + k_1k_2k_4k_5k_6 + k_1k_2k_3k_5k_6 + k_1k_2k_3k_4k_6 + k_1k_2k_3k_4k_5)$ and $V_2 = E_t(k_{-1}k_{-2}k_{-3}k_{-4}k_{-5}k_{-6})/(k_{-2}k_{-3}k_{-4}k_{-5}k_{-6} + k_{-1}k_{-3}k_{-4}k_{-5}k_{-6} + k_{-1}k_{-2}k_{-4}k_{-5}k_{-6} + k_3k_{-1}k_{-4}k_{-5}k_{-6})$ are the maximum velocities in forward and reverse directions, the Michaelis constants for A, B, P, Q, R are $K_A = (k_2k_3k_4k_5k_6)/(k_1k_2k_5k_6k_{-3} + k_1k_2k_4k_5k_6 + k_1k_2k_3k_5k_6 + k_1k_2k_3k_4k_6 + k_1k_2k_3k_4k_5)$, $K_B = (k_1k_5k_6k_{-2}k_{-3} + k_1k_4k_5k_6k_{-2} + k_1k_3k_4k_5k_6)/(k_1k_2k_5k_6k_{-3} + k_1k_2k_4k_5k_6 + k_1k_2k_3k_5k_6 + k_1k_2k_3k_4k_6 + k_1k_2k_3k_4k_5)$, $K_{AB} = (k_5k_6k_{-1}k_{-2}k_{-3} + k_4k_5k_6k_{-1}k_{-2} + k_{-1}k_3\ k_4k_5\ k_6)/(k_1k_2k_5k_6k_{-3} + k_1k_2k_4k_5k_6 + k_1k_2k_3k_5k_6 + k_1k_2k_3k_4k_6 + k_1k_2k_3k_4k_5)$, $K_P = k_{-1}k_{-2}k_{-3}k_{-4}k_{-5}/(k_{-2}k_{-3}k_{-4}k_{-5}k_{-6} + k_{-1}k_{-3}k_{-4}k_{-5}k_{-6} + k_{-1}k_{-2}k_{-4}k_{-5}k_{-6} + k_3k_{-1}k_{-4}k_{-5}k_{-6})$, $K_Q = k_{-1}k_{-2}k_{-3}k_{-4}k_{-6}/(k_{-2}k_{-3}k_{-4}k_{-5}k_{-6} + k_{-1}k_{-3}k_{-4}k_{-5}k_{-6} + k_{-1}k_{-2}k_{-4}k_{-5}k_{-6} + k_3k_{-1}k_{-4}k_{-5}k_{-6})$, $K_R = (k_{-1}k_{-2}k_{-3}k_{-5}k_{-6} + k_4k_{-1}k_{-2}k_{-5}k_{-6} + k_3k_4k_{-1}k_{-5}k_{-6})/(k_{-2}k_{-3}k_{-4}k_{-5}k_{-6} + k_{-1}k_{-3}k_{-4}k_{-5}k_{-6} + k_{-1}k_{-2}k_{-4}k_{-5}k_{-6} + k_3k_{-1}k_{-4}k_{-5}k_{-6})$, $K_{QR} = (k_5k_{-1}k_{-2}k_{-3}k_{-6} + k_4k_5k_{-1}k_{-2}k_{-6} + k_3k_4k_5k_{-1}k_{-6})/(k_{-2}k_{-3}k_{-4}k_{-5}k_{-6} + k_{-1}k_{-3}k_{-4}k_{-5}k_{-6} + k_{-1}k_{-2}k_{-4}k_{-5}k_{-6} + k_3k_{-1}k_{-4}k_{-5}k_{-6})$, $K_{PQ} = k_6k_{-1}k_{-2}k_{-3}k_{-4}/(k_{-2}k_{-3}k_{-4}k_{-5}k_{-6} + k_{-1}k_{-3}k_{-4}k_{-5}k_{-6} + k_{-1}k_{-2}k_{-4}k_{-5}k_{-6} + k_3k_{-1}k_{-4}k_{-5}k_{-6})$, $K_{PQR} = (k_5k_6k_{-1}k_{-2}k_{-3} + k_4k_5k_6k_{-1}k_{-2} + k_{-1}k_3\ k_4k_5\ k_6)/(k_{-2}k_{-3}k_{-4}k_{-5}k_{-6} + k_{-1}k_{-3}k_{-4}k_{-5}k_{-6} + k_{-1}k_{-2}k_{-4}k_{-5}k_{-6} + k_3k_{-1}k_{-4}k_{-5}k_{-6})$. The inhibition constants for A, B, P, Q, R are $K_{iA} = k_{-1}/k_1$, $K_{iB} = (k_{-2}k_{-3})/(k_2(k_{-3} + k_3))$, $K_{iP} = k_6/k_{-6}$, $K_{iQ} = k_5/k_{-5}$, $K_{iR} = (k_3k_4)/(k_{-4}(k_3 + k_{-3}))$. Use of the inhibition constants allows to redefine: $K_{PQ}=K_{iP}K_Q$ and $K_{QR}=K_{iQ}K_R$.

The equation 16 was employed to simulate the response curves and Eadie-Hofstee plots for the reagentless glutamate biosensors using the values of the Michaelis and inhibition constants found in the literature.[35]

Figure 8 demonstrates the effect of the value of maximum flux of the electrochemical oxidation of NADH (Γk_{cat}) on the simulated response of the reagentless glutamate biosensors (at A_t = 1 mM). The Eadie-

Hofstee plots yield the straight line characteristic for the process limited by the enzymatic reduction of NAD^+ only when Γk_{cat} is infinitively high. The decrease in the value of Γk_{cat} leads to the decrease in the values of intercepts of the Eadie-Hofstee plots with the axis of j and their negative slopes i.e. the apparent maximum current densities and apparent Michaelis constants, respectively, become lower due to the limitation set by the flux of the electrochemical oxidation of NADH. The decrease in the value of Γk_{cat} also effects the shape of Eadie-Hofstee plots making them more concave. Hence the concavity of Eadie-Hofstee plots is diagnostic for reagentless glutamate biosensors limited by the rate of electrochemical NADH oxidation at the electrode surface.

Figure 9 represents the effect of mass transport rate on the response of biosensors limited by the rate of the electrochemical NADH oxidation. The decrease in the mass transfer coefficients leads to the drastic increase in the slope of Eadie-Hofstee plots, making the apparent Michaelis constants (measured using high concentrations of glutamate) higher than K_B of free GLDH. It can be concluded that the concave Eadie-Hofstee plots, giving the values of apparent Michaelis constant higher than the value of K_M of the free enzyme, are diagnostic for the reagentless glutamate biosensors limited by the rate of electrochemical NADH oxidation at the electrode surface and by the rate of mass transport.

The effect of the maximum flux of the enzymatic reduction of NAD^+ (LV_1) rate on the response of biosensors limited by the rate of the electrochemical NADH oxidation and mass transport is illustrated in Figure 10. The increase in LV_1 leads to the drastic increase in apparent current densities and the concavity of the Eadie-Hofstee plots, making the apparent Michaelis constants higher than K_B of free GLDH.

The response curve of the glutamate biosensors is shown in Figures 11 and their basic characteristics obtained from the Eadie-Hofstee plots are represented in Table II. The Eadie-Hofstee plots (Figure 10(B)) show concavity characteristic for the process limited by the rate of NADH oxidation at the electrode surface. The value of the apparent Michaelis constant (47 mM) is significantly higher than the literature value of that for mesophilic bovine GLDH (2.5 mM)[35] implying that the response of these glutamate sensors is limited by the rate of electrochemical NADH oxidation and the mass transfer between the lamellar phase and the external solution.

The glutamate biosensors prepared using immobilization in the lamellar phase layers have very short operational half-life time (30 min) and long response time 7-8 min. The loss of the response was caused by leaching of NAD^+ from the electrode surface. This was proven by the injection of NAD^+ at the end of operational stability study (when one half of the initial response to glutamate and 20% of Os-phendione-PVP were lost according to the data obtained by cyclic voltammetry. The injection of NAD^+ lead to the recovery of c.a. 80 % of the initial response current demonstrated by the biosensors operated in the presence of NAD^+.

CONCLUSIONS

The new NADH oxidizing surfactant can be synthesized by complexation of [Os(1,10-phenanthroline-5,6-dione)$_2$Cl$_2$] with hydrophobic ligand and can be used for the formation of the aqueous lamellar phase which entraps NAD^+ dependent glutamate dehydrogenase and NAD^+. The resulting lamellar phase suspension can be

immobilized by adsorption on graphite electrodes to yield reagentless glutamate biosensors operating at 150 mV *vs.* Ag/AgCl/KCl_{sat}. Their response is limited by the rate of electrochemical NADH oxidation and the mass transfer between the lamellar phase and the external solution. Their low operational stability is determined by leaching of NAD^+.

ACKNOWLEDGEMENTS

This paper was supported by the grants of European Community, Industrial & Material Technologies Programme (Brite-EuRam III), project No. BE97-4511, the Spanish Ministry of Education and Culture Ref.: Acciones Especiales MAT98-1413.CE. V.P. acknowledges Ph. D. fellowship and the special grant Ref.:M3C99-80 from the Department of chemical engineering, University Rovira I Virgili.

LEGEND TO TABLE

Table I. Basic characteristics of the reagentless glutamate biosensors calculated from the Eadie-Hofstee plot.

LEGENDS TO FIGURES

Figure 1. Schematic diagram of the electron transfer steps for the mediated glutamate biosensors.

Figure 2. Synthetic route to the NADH oxidising tensoactive mediator Os-phendione-surfactant.

Figure 3. Surface pressure/area isotherm for Os-phendione-surfactant.

Figure 4. Cyclic voltammograms of reagentless glutamate biosensors based on the lamella phase layers and GLDH in the absence of glutamate and the presence 0.35 M glutamate**.** Scan rate 0.3 mV s^{-1}. Experimental conditions: E_{app} 150 mV *vs.* Ag/AgCl/KCl_{sat}, 0.1 M phosphate buffer (pH 7.4), temperature 30°C.

Figure 5. Effect of pH on maximum response of reagentless glutamate biosensors based on the lamellar phase. Experimental conditions: E_{app} 150 mV *vs.* Ag/AgCl/KCl_{sat}, 0.1 M phosphate buffer, temperature 30°C.

Figure 6. Effect of temperature on maximum response of reagentless glutamate biosensors based on the lamellar phase. Experimental conditions: E_{app} 150 mV *vs.* Ag/AgCl/KCl_{sat}, 0.1 M phosphate buffer (pH 7.4).

Figure 7. Reaction scheme for a reagentless glutamate biosensor.

Figure 8. Simulation of the Eadie-Hofstee plots for the reagentless glutamate biosensors with varying maximum fluxes of the electrochemical NADH oxidation (Γk_{cat}): a) 2.6×10^{-11} mol s^{-1} cm^{-2}; b) 1.04×10^{-10} mol s^{-1} cm^{-2};

c) 4.15x10^{-10} mol s^{-1} cm^{-2}; d) 8.3x10^{-10} mol s^{-1} cm^{-2}; e) 1.7x10^{-9} mol s^{-1} cm^{-2}; f) 1.3x10^{-8} mol s^{-1} cm^{-2}; g) 5.178x10^{-8} mol s^{-1} cm^{-2}; h) ∞. The values of other parameters are: A_t=1 mM; $k'_B \rightarrow \infty$; $k'_Q \rightarrow \infty$; $k'_R \rightarrow \infty$; LV_1=3.63x10^{-10} mol s^{-1} cm^{-2}; K_M = 0.8 mM; K_A = 0.23 mM; K_B = 2.5 mM; K_{AB} = 0.3 mM^2; K_{iA} = 10 mM; K_{iB} = 11 mM; K_R = 20 mM; K_Q = 0.25 mM; K_P = 0.04 mM; K_{iR} = 9 mM; K_{iQ} = 1.6 mM; K_{iP} = 0.03 mM.

Figure 9. Simulation of the Eadie-Hofstee plots for the reagentless glutamate biosensors with varying mass transfer coefficients (k'_B, k'_Q, k'_R): a) 5.18x10^{-12} cm s^{-1}; b) 2.6x10^{-11} cm s^{-1}; c) 5.18x10^{-11} cm s^{-1}; d) 1.03x10^{-10} cm s^{-1}; e) 2.6x10^{-10} cm s^{-1}; f) ∞. ∞. The values of other parameters are: A_t=1 mM; LV_1 = 3.63x10^{-10} mol s^{-1} cm^{-2}; Πk_{cat} = 8.3x10^{-10} mol s^{-1} cm^{-2}; K_M = 0.8 mM; K_A = 0.23 mM; K_B = 2.5 mM; K_{AB} = 0.3 mM^2; K_{iA} = 10 mM; K_{iB} = 11 mM; K_R = 20 mM; K_Q = 0.25 mM; K_P = 0.04 mM; K_{iR} = 9 mM; K_{iQ} = 1.6 mM; K_{iP} = 0.03 mM.

Figure 10. Simulation of the Eadie-Hofstee plots for the reagentless glutamate biosensors with varying maximum flux of enzymatic reduction of NAD$^+$ (LV_1): a) 1.55x10^{-10} mol s^{-1} cm^{-2}; b) 3.63x10^{-10} mol s^{-1} cm^{-2}; c) 6.22x10^{-10} mol s^{-1} cm^{-2}; d) 1.24x10^{-9} mol s^{-1} cm^{-2}; e) 2.49x10^{-9} mol s^{-1} cm^{-2}. The values of other parameters are: k'_B =2.6x10^{-11} cm s^{-1}; k'_Q =2.6x10^{-11} cm s^{-1}; k'_R =2.6x10^{-11} cm s^{-1}; A_t=1 mM; Πk_{cat} = 8.3x10^{-10} mol s^{-1}cm^{-2}; K_M = 0.8 mM; K_A = 0.23 mM; K_B = 2.5 mM; K_{AB} = 0.3 mM^2; K_{iA} = 10 mM; K_{iB} = 11 mM; K_R = 20 mM; K_Q = 0.25 mM; K_P = 0.04 mM; K_{iR} = 9 mM; K_{iQ} = 1.6 mM; K_{iP} = 0.03 mM.

Figure 11. Dependence of the steady apparent current density on L-glutamate concentration **(A)** and the Eadie-Hofstee plots **(B)** for reagentless biosensors based on the lamellar phase. Experimental conditions: E_{app} 150 mV *vs.* Ag/AgCl/KCl$_{sat}$, 0.1 M phosphate buffer (pH 7.4), temperature 30°C.

REFERENCES

(1) Sprintschik, G.; Sprintschik, H. W.; Kirsch, P. P.; Whitten, D. G. *J. Am. Chem. Soc.* **1976**, *98*, 2337-2338.

(2) Gaines, G. L.; Behnken, P. E.; Valenty, S. J. *J. Am. Chem. Soc.* **1978**, *100*, 6549-6559.

(3) Saudan, P.; Zakeeruddin, S. M.; Malavallon, M. A.; Grätzel, M.; Fraser, D. M. *Biotechnol. Bioengin.* **1994**, *44*, 407-418.

(4) Zakeeruddin, S. M.; Grätzel, M.; Fraser, D. M. *Biosens. Bioelectron.* **1996**, *11*, 305-315.

(5) Fraser, D. M.; Zakeeruddin, S. M.; Grätzel, M. *Biochim. Biophys. Acta* **1992**, *1099*, 91-101.

(6) Ryabov, A. D.; Amon, A.; Gorbatova, R. K.; Ryabova, E. S.; Gnedenko, B. B. *J. Phys. Chem.* **1995**, *99*, 14072-14077.

(7) Sackmann, E. *Science,* **1996**, *271*, 43-48.

(8) Miller, C.; Cuendet, P.; Grätzel, M. *J. Electroanal. Chem.* **1990**, *278*, 175-192.

(9) Florin E. L.; Gaub, H. E. *Biophys. J.* **1993,** *64*, 375-383.

(10) Kuhn, H.; Möbius H. D.; Bücher, H. In *Physical Methods of Chemistry*, Part IIIB, Weissenberger, A.; Rossiter, B. M. Eds.; Wiley: New York, 1972; pp. 577-578.

(11) Egger, M.; Heyn, S. P.; Gaub, H. E. *Biophys. J.* **1990**, *57*, 669-673.

(12) Kalb, E.; Frey, S.; Tamm, L. K. *Biochim. Biophys Acta* **1992** , *1103*, 307-316.

(13) Bayerl, Th. M.; Bloom, M. *Biophys. J.* **1990**, *58*, 357-362.

(14) Duschl, C.; Liley, M.; Lang, H.; Ghandi, A.; Zakeeruddin, S. M.; Stahlberg, H.; Dubochet, J.; Nemetz, A.; Knoll, W.; Vogel, H. *Mater. Sci. Eng. C* **1996**, *4,* 7-18.

(15) Salamon, Z.; Hazzard, J. T.; Tollin, G. *Proc. Natl. Acad. U.S.A.* **1993**, *90*, 6420-6423.

(16) Lindholm-Sethson, B.; Gonzalez, J. C.; Puu, G. *Langmuir* **1998**, *14*, 6705-6708.

(17) Naumann, R.; Schmidt, E. K.; Jonczyk, A.; Fendler, K.; Kadenbach, B.; Liebermann, T.; Offenhäusser, A.; Knoll, W. Biosens. *Bioelectron.* **1999**, *14*, 651-662.

(18) Bunjes, N.; Schmidt, E. K.; Jonczyk, A.; Rippmann, F.; Beyer, D.; Ringsdorf, H.; Gräber, P.; Knoll, Naumann, W.; R. *Langmuir*, **1997**, *13*, 6188-6194.

(19) Schmidt, E. K.; Liebermann, T.; Kreiter, M.; Jonczyk, A.; Naumann, R.; Offenhäuser, A.; Neumann, E.; Kukol, A.; Maelicke, A.; Knoll, W. *Biosens. Bioelectron.* **1998**, *13*, 585-591.

(20) Taylor, M. A.; Jones, M. N.; Vadgama, P.; Higson, S. P. J. *Biosens. Bioelectron.* **1995**, *10*, 251-260.

(21) Taylor, M. A.; Jones, M. N.; Vadgama, P.; Higson, S. P. J. *Biosens. Bioelectron.* **1997**, *12*, 467-477.

(22) Engelsen, B. *J. Neurochem.* **1986**, *47*, 1634-1641.

(23) Greenamyre, J. T. *Arch. Neurol.* **1986**, *43*, 1058-1063.

(24) Rietz, B.; Guilbault, G. G. *Anal. Chim. Acta 77*, **1975**, 191-198.

(25) Amouyal, E.; Homsi, A.; Chambron, J.-C.; Sauvage, J.-P. *J. Chem. Soc., Dalton Trans.* **1990**, 1841-1845.

(26) Lay, P. A.; Sargeson, A. M.; Taube, H. In *Inorganic Synthesis*; Shreeve J. M., Ed.; John Wiley: New York, 1986; Vol 24; pp. 293-295.

(27) Wu, Q.; Maskus, M.; Pariente, F.; Tobalina, F.; Fernandez, V. M.; Lorenzo, E.; Abruña, H. D. *Anal. Chem.* **1996**, 68, 3688-3696.

(28) Goss, C. A.; Abruña, H. D. *Inorg. Chem.* **1985**, *24*, 4263-4267.

(29) Popescu, I. C.; Dominguez, E.; Narvaez, A.; Pavlov, V.; Katakis, I. *J. Electroanal. Chem.* **1999**, 464, 208-214.

(30) Pavlov, V.; Rincón, O.; Solé, S.; Narváez, A.; Domínguez, E.; Katakis I. Submitted to *Anal. Chem.*

(31) Smith, E. L.; Austen, B. M.; Blumenthal, M. K.; Nyc, J. F. In *The Enzymes*; Boyer, P. D., Ed.; Academic Press: New York, 1975, volume XI, pp. 359-360.

(32) Yamamura, A.; Sakaguchi, T.; Murakami, Y.; Yokoyama, K.; Tamiya, E. *Biochem. J.* **1999**, *125*, 760-769.

(33) O'Flaherty, M.; McMahon, M.; Forde, J.; Mulcahy, P. *Prot. Express. Purif.* **1999**, 16, 276-297.

(34) Albery, W. J.; Bartlett, P. N.; Cass, A. E. G.; Sim, K. W. *J. Electroanal. Chem.* **1987**, *218*, 127-134.

(35) Fahien, L. A.; Strmecki, M. *Arch. Biochem. Biophys.* **1969**, *130*, 468-477.

Table I

J_{max}, μA cm^{-2}	RSD, %	Response time, s	K_M, mM	Operational half-life time, h
3.5	25.0	220	47	0.5

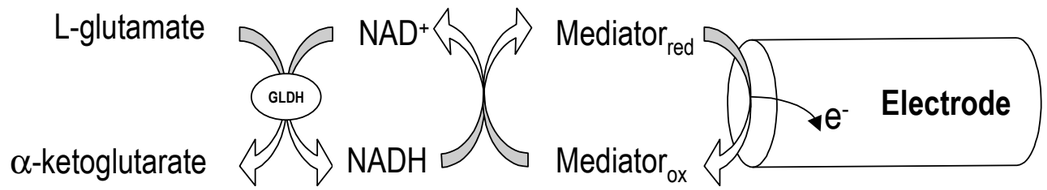
L-glutamate
α-ketoglutarate
GLDH
NAD+
NADH
Mediator red
Mediator ox
e-
Electrode

Figure 1

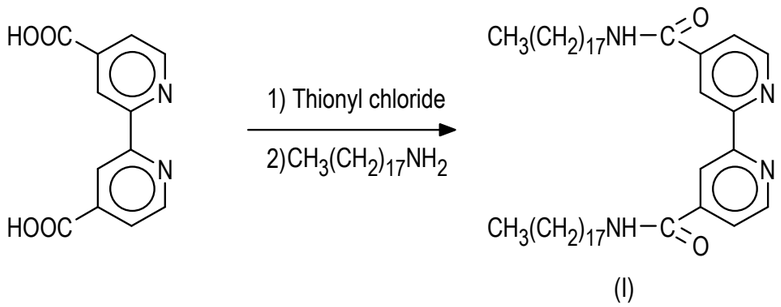
HOOC
N
N
HOOC
1) Thionyl chloride
2)CH3(CH2)17NH2
CH3(CH2)17NH—C
O
N
N
CH3(CH2)17NH—C
O

(I)

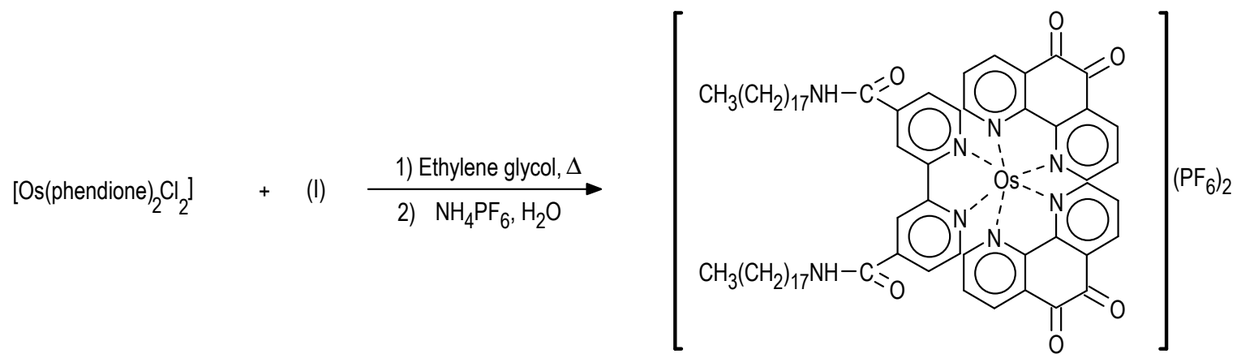
[Os(phendione)2Cl2]
+
(I)
1) Ethylene glycol, Δ
2) NH4PF6, H2O
CH3(CH2)17NH—C
O
N
N
Os
N
N
N
N
CH3(CH2)17NH—C
O
O
O
O
O
(PF6)2

(II)

Figure 2

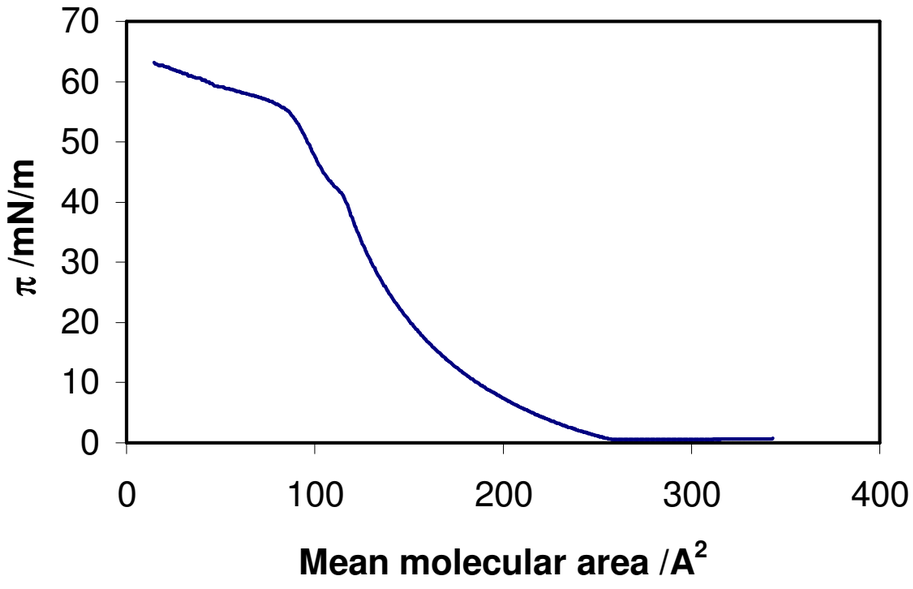
70
60
50
40
30
20
10
0
π /mN/m
0
100
200
300
400
Mean molecular area /A2

Figure 3

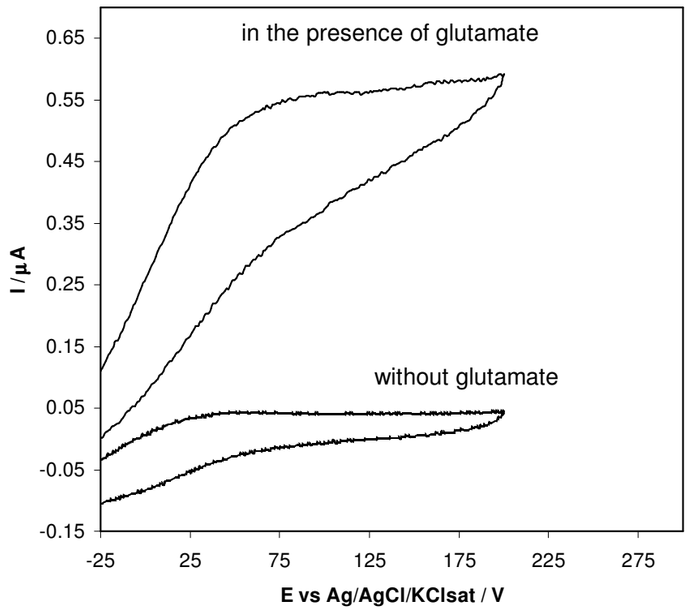
in the presence of glutamate
without glutamate
0.65
0.55
0.45
0.35
0.25
0.15
0.05
-0.05
-0.15
-25
25
75
125
175
225
275
I / µA
E vs Ag/AgCl/KClsat / V

Figure 4

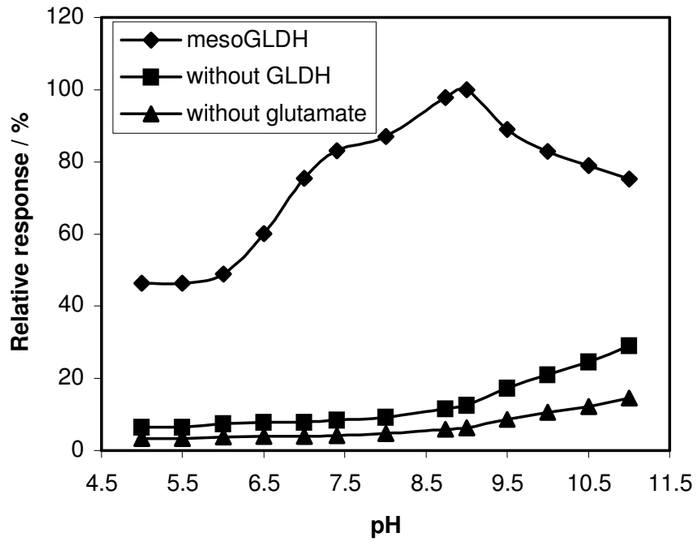
120
100
80
60
40
20
0
4.5
5.5
6.5
7.5
8.5
9.5
10.5
11.5
pH
Relative response / %
mesoGLDH
without GLDH
without glutamate

Figure 5

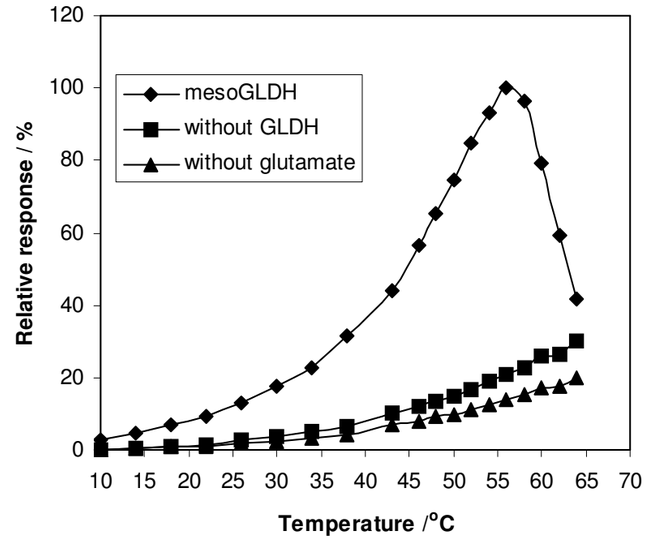
120
100
80
60
40
20
0
Relative response / %
10 15 20 25 30 35 40 45 50 55 60 65 70
Temperature /°C
mesoGLDH
without GLDH
without glutamate

Figure 6

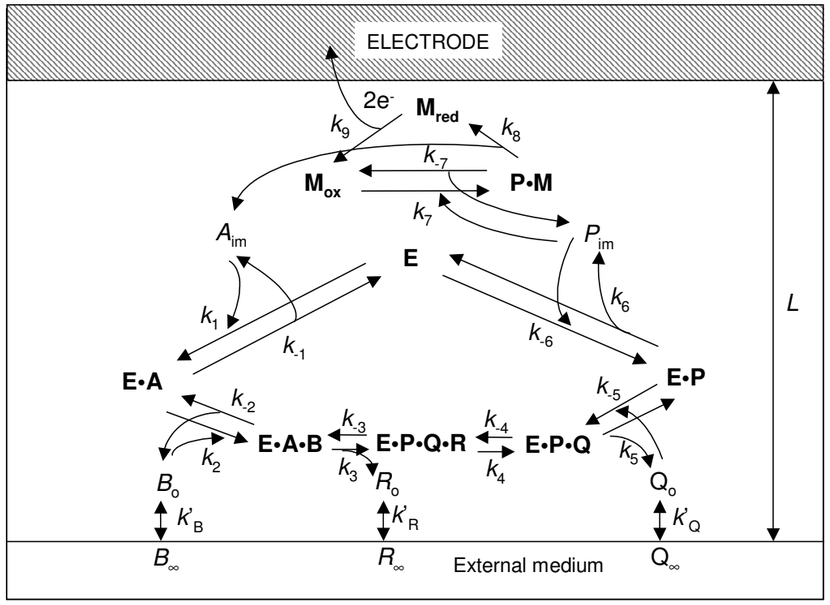
ELECTRODE
2e-
M_{red}
k_9
k_8
k_{-7}
M_{ox}
P•M
k_7
A_{im}
P_{im}
E
k_1
k_{-1}
k_6
k_{-6}
L
E•A
E•P
k_{-2}
k_{-5}
k_{-3}
k_{-4}
E•A•B
E•P•Q•R
E•P•Q
k_2
k_3
k_4
k_5
B_o
R_o
Q_o
k'_B
k'_R
k'_Q
B_∞
R_∞
External medium
Q_∞

Figure 7

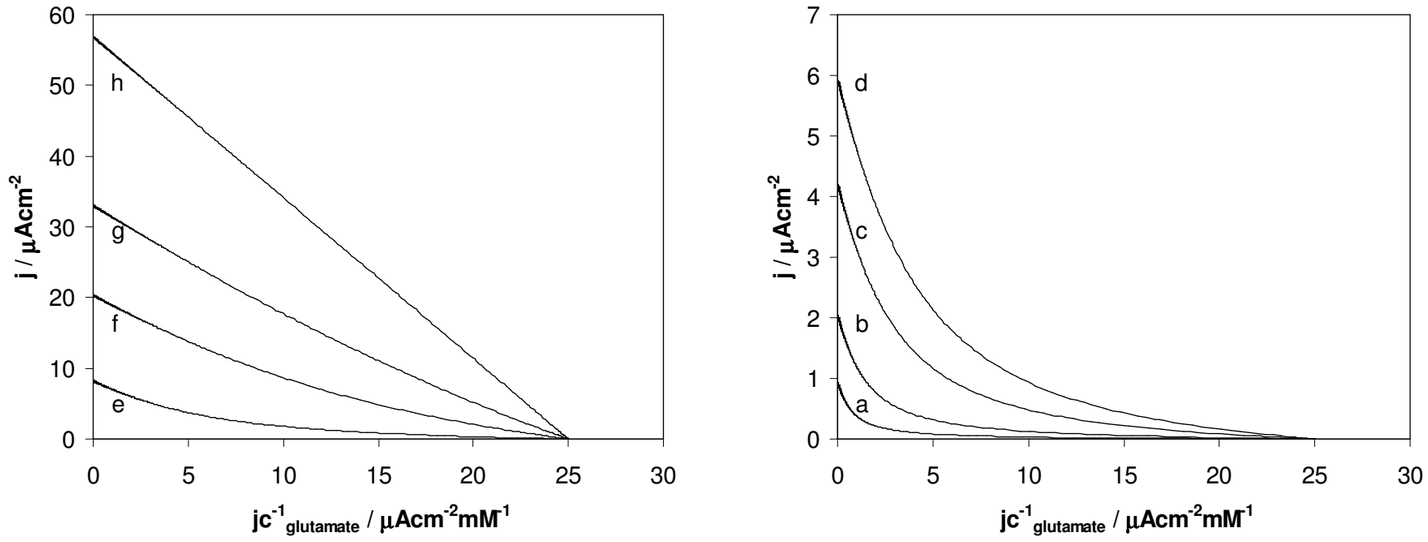
60
50
40
30
20
10
0
h
g
f
e
j / µAcm-2
0
5
10
15
20
25
30
jc-1glutamate / µAcm-2mM-1
7
6
5
4
3
2
1
0
d
c
b
a
j / µAcm-2
0
5
10
15
20
25
30
jc-1glutamate / µAcm-2mM-1

Figure 8

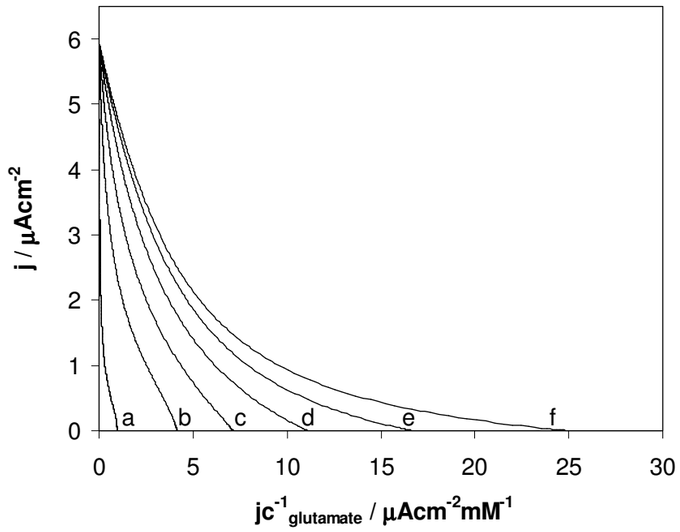
j / µAcm-2
6
5
4
3
2
1
0
a
b
c
d
e
f
0
5
10
15
20
25
30
jc-1glutamate / µAcm-2mM-1

Figure 9

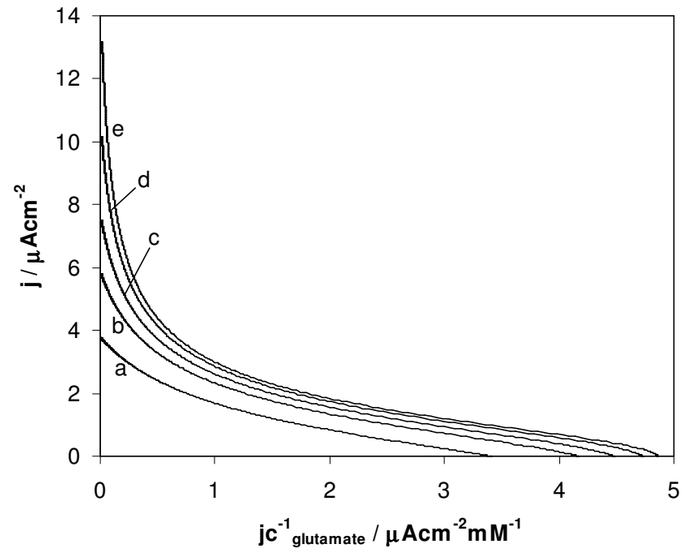

Figure 10

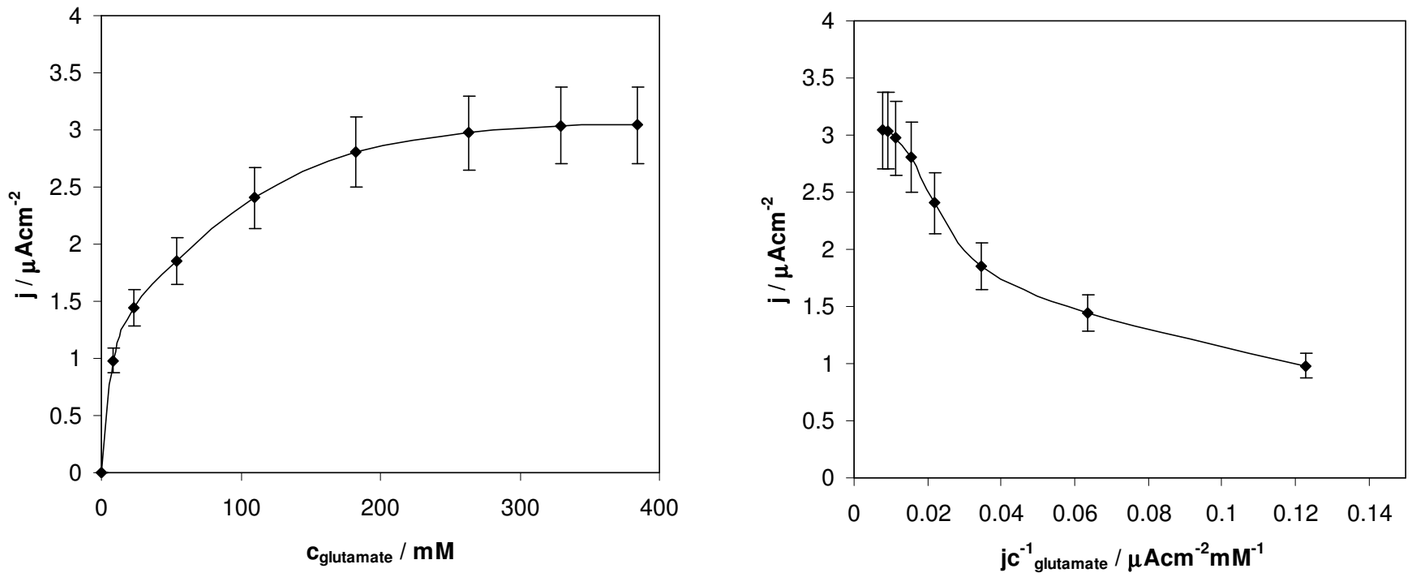

(A) **(B)**

Figure 11